Int. J. Electrochem. Sci., 12 **(2017)** 2593 – 2605, doi: 10.20964/2017.03.10

International Journal of
ELECTROCHEMICAL
SCIENCE
www.electrochemsci.org

Effect of Rotating Speed and Hydrostatic Pressure on Erosion-Corrosion Behavior of X65 Pipeline Steel

Qiongbin Zheng, Liuyan Zhang[*]*, Xiaohua Jie*[*]*, Xiaoye Huang, Song Luo*

School of Materials and Energy, Guangdong University of Technology, Guangzhou 510006, PR China
[*]E-mail: zlyjust@gdut.edu.cn (Liuyan Zhang); cnxyyz3@gdut.edu.cn (Xiaohua Jie)

Received: 30 November 2016 / *Accepted:* 8 January 2017 / *Published:* 12 February 2017

A simple rotating experimental setup with adjustable rotating speed and hydrostatic pressure was established to simulate the erosion-corrosion environment. The effect of rotating speed and hydrostatic pressure on the erosion-corrosion behavior of X65 steel in 3.5 mass% NaCl was investigated by polarization, electrochemical impedance spectroscopy, and scanning electron microscopy. The results revealed that the rotating speed changed the corrosion type of X65 steel from a pure uniform electrochemical corrosion into the combination of uniform corrosion and local damage, which was aggravated with increasing the rotating speed. The hydrostatic pressure has the opposite effect on the uniform and local corrosion of X65 steel, showing a decrease of uniform corrosion and an increase of local damage.

Keywords: X65 steel; rotating speed; hydrostatic pressure; erosion-corrosion; local damage

1. INTRODUCTION

Erosion-corrosion (E-C) of marine pipeline steels in flowing environment is a major issue, which results in a great degradation of metal surface and a large damage of the oil and gas transportation system in seawater [1]. In flowing condition, the protective oxide film of metal is disrupted, which results in the increase of oxygen and the acceleration of corrosion [2]. Furthermore, the erosion-corrosion occurs the synergistic effects of corrosion and wear, which is complex electrochemical and mechanical mechanisms, causing a higher damage of the metal surface than the sum of pure corrosion and pure erosion [3, 4]. Therefore, in order to have a better understanding of the reasonable selection and application of the metals in the corrosion-erosion environment, during the past few decades, various studies have been carried out to characterize material corrosion and erosion resistance under different condition [5].

Researches on the erosion-corrosion indicate that diverse factors such as rotating speed, materials, temperature, hydrostatic pressure, etc., Which are responsible for the initiation and

propagation of the corrosion. Tian et al [6, 7] reported that the corrosion of X65 steel increased with the increasing electrode rotating speed, the presence of sand particles increased the anodic dissolution current density and decreased the corrosion potential negatively. The addition of oil decreased the dissolution of X65 steel due to a layer of oily phase forms on steel surface [8]. Hu et al. [9] investigated the erosion-corrosion behavior of stainless steel and discovered that its weight loss increased markedly when the temperature increased from 18 ^{o}C to 50 ^{o}C. Hamdy et al. [10] studied the electrochemical response and erosion-corrosion of mild steel in the aerated sulfide containing 3.5 mass% NaCl solutions, and revealed that the presence of sulfide ions significantly decreased the corrosion resistance of mild steel.

Hydrostatic pressure is specifically characterized in the deep ocean environment, it has been claimed that hydrostatic pressure was a significant factor to material corrosion [11, 12]. The effect of hydrostatic pressure on nickel alloy was reported by Beccaria et al. [13], showing that the corrosion rate and susceptibility of pitting increased with increasing the hydrostatic pressure. Sun [14] investigaed the corrosion of low alloy steel in NaCl solution at high hydrostatic pressure, and found out the initiation rate and planar growth of the localized corrosion were both promoted. However, the effect of hydrostatic pressure was mostly studied under static condition. There was little information available on the erosion-corrosion behavior under hydrostatic pressure environment. X65 pipeline steel as high strength low alloy steel is widely used for oil and gas transportation system in deep sea, but its erosion-corrosion behavior under different rotating speed and hydrostatic pressure is rarely reported.

In the present work, a simple rotating experimental setup with adjustable rotating speed and hydrostatic pressure will be established to simulate the erosion-corrosion environment under different erosive force and pressure. The X65 pipeline steel is prepared and the effect law of rotating speed and hydrostatic pressure on its erosion-corrosion behavior will be revealed.

2. EXPERIMENTAL DETAILS

2.1. Material

An X65 pipeline steel is used as the raw material and its chemical composition (wt.%) is listed in Table 1. The specimens with dimensions of 10 mm × 15 mm × 4 mm were cut from the raw material and prepared for erosion-corrosion tests. Before test, the samples were embedded in epoxy resin with an exposed area of 1.5 cm^2. The working surface was ground successively with 220, 400, 600, 800 and 1000 grit silicon carbide papers, cleaned by distilled water, degreased with acetone, dried and placed in a desiccator. All the experiments were conducted in a 3.5 mass% NaCl solution at room temperature (25±1^{o}C).

Table 1. Chemical composition of X65 pipeline steel (wt.%).

C	Si	Mn	Ni	Cr	Ti	V	Mo	Nb	Fe
0.04	0.16	1.47	0.13	0.18	0.013	0.004	0.001	0.041	Bal.

2.2. Experimental equipment

The experimental setup was designed by the authors for simulating the erosion-corrosion behaviors of X65 steel under hydrostatic pressure, which is schematically shown in Fig. 1. The stirrer was fixed in the autoclave and the specimens were fixed on the edge of the vessel. The angular speed (ω) of the stirrer was regulated by the rotate speed controller and the rotating speed was adjusted in the range of 0-400 rpm. And the hydrostatic pressure was controlled by filling the nitrogen gas into the pressure autoclave to apply a hydrostatic pressure upon the 3.5 mass% NaCl solution [15, 16]. The temperature was measured by a thermocouple and controlled by a thermostatic bath to room temperature.

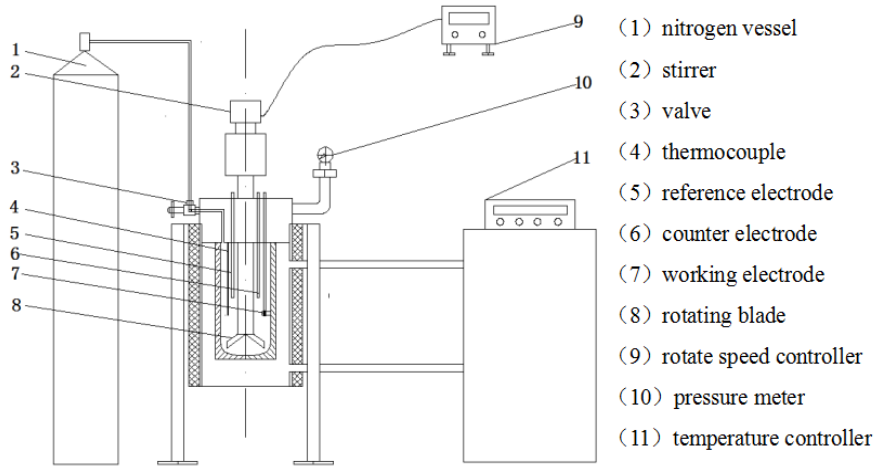

Figure 1. Schematic diagram of the experimental setup.

2.3. Electrochemical measurement

The electrochemical tests were carried out on a CHI660E electrochemical analyzer (shanghai, China) with a three-electrode cell. X65 steel sample was used as a working electrode, the reference electrode was a saturated calomel electrode (SCE) and platinum as counter electrode.

Prior to electrochemical measurements, the sample was immersed in 3.5 mass% NaCl for 12 h at different rotating speeds and different hydrostatic pressures, and then the electrodes were in the test solution for at least 1 h until the open circuit potential was steady.

In the potentiodynamic polarization curves measurement, the tests were performed in the applied potential range from -1300 mV to -400 mV at a sweep rate of 0.333 mV/s. The curves were fitted and analyzed with CHI660E electrochemical analyzer, and the corrosion rates were evaluated with polarization resistance values obtained by linear polarization [17].

Electrochemical impedance spectroscopy (EIS) tests were carried out at the open-circuit potential, over a frequency range of 10^5 Hz to 10^{-2} Hz with a single amplitude perturbation of 5 mV. The EIS curves were analyzed and fitted to equivalent circuits by using the software ZsimpWin. All electrochemical measurements were conducted at least three times to confirm reproducibility.

2.4. Surface analysis

The microscopic corrosion morphology of samples after immersed in 3.5 mass% NaCl for 12 h in different corrosion tests were observed by scanning electron microscopy (SEM). Elemental analysis of corroded surface was conducted using energy dispersive spectrometer (EDS).

3. RESULTS AND DISCUSSION

3.1. Microstructure

Figure 2 shows the microstructure of X65 pipeline steel sample. As shown in Fig. 2, the microstructure of the X65 pipeline steel consists of pearlite of about 5 vol.% (dark phase) and the remainder of ferrite (bright phase) with the average grain size of about 10 μm; the pearlite lumps show the random distribution characteristics.

From the chemical composition of the X65 pipeline steel (Table 1), the fine structure of the X65 pipeline steel can be due to its composition containing low quantities of niobium, titanium, and vanadium elements, which can refine grains [18].

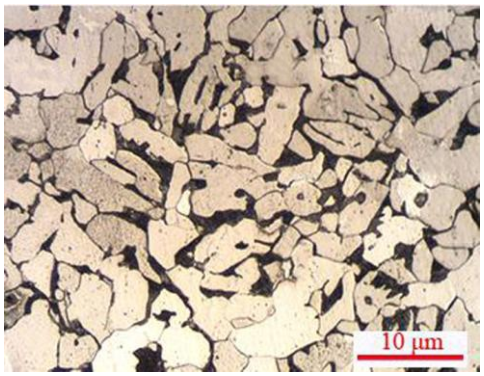

Figure 2. Microstructure of X65 pipeline steel.

3.2. Effect of rotating speed on erosion-corrosion at atmospheric pressure

Figure 3 shows the polarization curves of X65 steel after 12 h of immersion in 3.5 mass% NaCl solution at atmospheric pressure with different rotating speeds. As shown in Fig. 3, the different polarization curves are in a similar shape, but their positions are not same. The polarization kinetic parameters including the corrosion potential (E_{corr}), corrosion current density (i_{corr}), anodic Tafel slope (β_α) and cathodic Tafel slope (β_c) were calculated by using the Tafel extrapolation method [21], which are listed in Table 2.

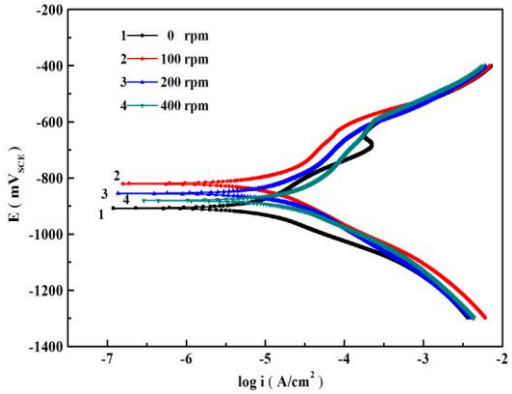

Figure 3. Polarization curves of X65 steel after 12 h of immersion in 3.5 mass% NaCl solution at atmospheric pressure with different rotating speeds.

Table 2. Electrochemical parameters of X65 steel after erosion-corrosion with different rotating speeds.

Rotating speed (rpm)	E_{corr} (mV_{SCE})	i (10^{-6} A/cm^2)	R_p (Ω cm)	Corrosion rate (mm/y)	β_α (mV/ decade)	βc (mV/ decade)
0	-908	15.27	1825.4	0.177	171.4	102.4
100	-821	21.45	1761.5	0.249	175.9	123.5
200	-855	26.36	1346.4	0.306	203.1	138.2
400	-880	35.77	919.3	0.415	233.9	152.3

As shown in Table 2, it can be obviously seen that the i_{corr} and corrosion rate values increase and the R_p values decrease with increasing the rotating speed. When the rotating speed was higher than 0 rpm, the E_{corr} values of the samples gradually shifted in negative direction with increasing the rotating speed, which were still more positive than that of the sample in the static condition. A similar change law of the corrosion potential under rotational flow and static condition was also observed by Tian [6] and Zheng [20].

The difference in corrosion potential of the samples under different rotating speeds was explained from the point of corrosion products by Zheng [20]. Compared to the rotational flow environment, the destructive power of static immersion environment was lower. The corrosion products on the samples under static immersion environment were attached to the sample surface, and a series of complex reaction happened to form the products of α-, β-, γ-FeOOH, α-, γ-Fe_2O_3, Fe_3O_4 and amorphous oxyhydroxides, which were not dense causing the corrosion potential more negatively.

As shown in Fig. 3 and Table 2, it is observed that the slope of cathodic polarization segment increases with increasing the rotating speed, which indicates that the cathodic reaction (oxygen reduction) is accelerated. The acceleration of cathodic reaction could be attributed to the enhanced transfer rate of dissolved oxygen [8]. Furthermore, under dynamic condition, the corrosion products were easily removed by the flowing solution, which also accelerated the anodic reaction by promoting

the metal substrate Fe dissolve into metallic ion Fe^{2+} [20]. The β_α values in Table 2 increased when the corrosion condition turned from static state to dynamic state. The reaction occurred in the neutral NaCl solution under dynamic state are shown in equations 1 to 3.

Anodic reaction: $Fe_{(s)} \rightarrow Fe^{2+}_{(ac)} + 2e^-$ (1)

Cathodic reaction: $O_{2(g)} + 2H_2O_{(l)} + 4e^- \rightarrow 4OH^-_{(ac)}$ (2)

Total reaction: $2Fe_{(s)} + O_{2(g)} + 2H_2O_{(l)} \rightarrow 2Fe^{2+}_{(ac)} + 4OH^-_{(ac)}$ (3)

Figure 4 shows the corrosion morphology of X65 steel after 12 h of immersion in 3.5 mass% NaCl solution at atmospheric pressure with different rotating speeds. It could be seen that the corrosion degree of the samples under different rotating speeds were different. As shown in Fig. 4a, the sample under static state corrosion shows uniform corrosion. When the rotating speed of the corrosion medium increased, the pitting corrosion phenomenon appeared along with the uniform corrosion. As shown in Figs. 4a-4d, the number and size of the corrosion pits increased significantly with rotating speed (marked by the arrows). Under erosion-corrosion environment, the damage form of the sample surface is a combination of uniform corrosion and local failure due to the synergy effect between the electrochemical corrosion and washing force.

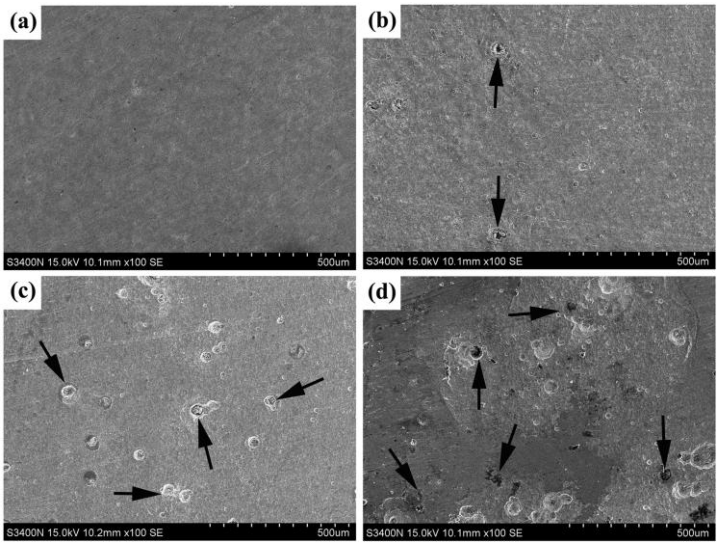

Figure 4. SEM morphologies of of X65 steel after 12 h of immersion in 3.5 mass% NaCl solution at atmospheric pressure with different rotating speeds: (a) 0 rpm; (b) 100 rpm; (c) 200 rpm; (d) 400 rpm.

Figure 5 shows the EIS curves of X65 steel after 12 h of immersion in 3.5 mass% NaCl solution at atmospheric pressure with different rotating speeds, which are detailed in Nyquist plot, and Bode phase angle plots. As shown in Figs. 5a, the impedance value in the low frequency decreased with increasing the rotating speed. As shown in Figs. 5b, the sample under static immersion environment obviously behaves one time constant (marked by the arrow A), which indicates that its Nyquist plot has one single capacitive arc. The samples under erosion-corrosion with a constant

rotating speed have two time constants (marked by the arrows B), which indicates their Nyquist plots have double capacitive arcs.

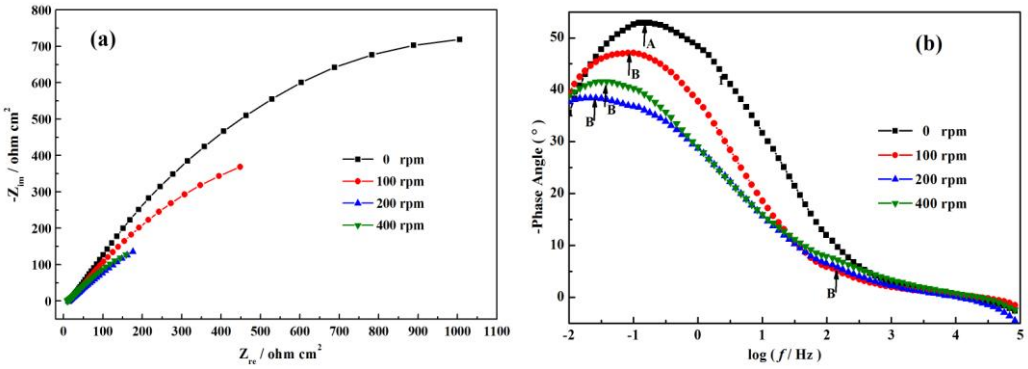

Figure 5. EIS curves of X65 steel after 12 h of immersion in 3.5 mass% NaCl solution at atmospheric pressure with different rotating speeds: (a) Nyquist plot; (b) Bode phase angle plot.

Combining with the analysis of the damage form and Nyquist plots, the equivalent circuit models of the different samples can be given, which are shown in Fig. 6. The sample under static immersion corrosion occurred uniform corrosion, and its Nyquist plot behaved one single capacitive arc. Thus, the equivalent circuit model of the Nyquist plot for the sample under static immersion corrosion can be described as $R_s(Q_{dl}R_t)$, where R_s is the solution resistance, R_t is the charge transfer resistance of the uniform corrosion, Q_{dl} is the constant phase element.

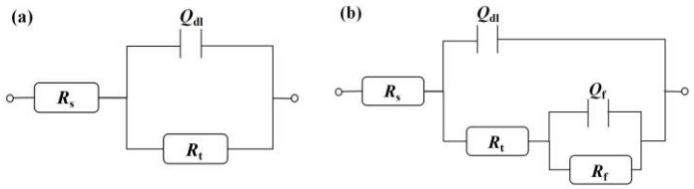

Figure 6. Equivalent circuits of the samples under different conditions: (a) static immersion environment; (b) erosion-corrosion with a constant rotating speed.

The sample under erosion-corrosion with a constant rotating speed occurred uniform corrosion accompanied with pitting corrosion, and its Nyquist plot behaved double arcs. Thus, as shown in Fig. 6b, the equivalent circuit model of the Nyquist plot for the sample under erosion-corrosion can be described as $R_s(Q_{dl}(R_t(Q_fR_f)))$, where R_s is the solution resistance, R_t is the charge transfer resistance of the uniform corrosion, Q_{dl} and Q_f is the constant phase element, R_f is the charge transfer resistance of the pitting corrosion.

Table 3 shows the R_t and R_f values fitted by using ZSimpWin software. The lower R_t means the higher uniform corrosion rate of the whole surface. The lower R_f means the higher pitting corrosion rate of the local surface. As shown in Table 3, the R_t value of the sample under static immersion

corrosion is about 4618 ohm cm^2, while its R_f value can be ignored due to the sample mainly occur uniform corrosion. Under erosion-corrosion, the R_t value of the sample decreases with increasing the rotating speed, which indicates the additional washing force accelerates uniform corrosion. The sample under erosion-corrosion environment occurred local damage. The R_f value representing pitting resistance of the sample decreased with increasing the rotating speed, which indicates the additional washing force accelerates pitting corrosion of X65 steel.

Table 3. EIS parameters of the samples under different rotating speeds.

Rotating speed（rpm）	R_t (ohm cm^2)	R_f (ohm cm^2)
0	4618	—
100	1498	778
200	1109	15.2
400	942	13

When non erosive force is applied, X65 steel immersed in the 3.5 mass% NaCl solution occurs pure electrochemical corrosion. When a certain erosive force is applied on the steel, the synergistic effect of erosive force and corrosive attack causes the aggravated uniform corrosion and local damage.

3.3. Effect of hydrostatic pressure on erosion-corrosion

Figure 7 shows the potentiodynamic polarization curves of X65 steel samples under erosion-corrosion environment with a rotating speed of 100 rpm at different hydrostatic pressures in 3.5 mass% NaCl solution at room temperature (25°C). It can be seen that the change of hydrostatic pressure significantly affects the electrochemical corrosion behavior of the samples after washing of a dynamic flow. The curves of the samples under erosion-corrosion was obviously shifted to left, which indicates their corrosion current decreased.

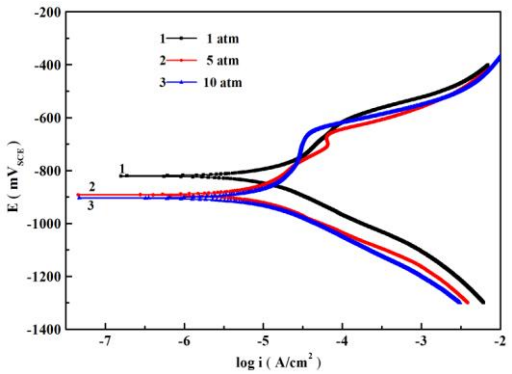

Figure 7. Polarization curves X65 steel after 12 h of erosion-corrosion in 3.5 mass% NaCl solution at different hydrostatic pressures.

Table 4 shows free corrosion potential (E_{corr}), free corrosion current density (i_{corr}), polarization resistance (R_p), anodic Tafel slope (β_α) and cathodic Tafel slope (β_c). It could be seen that the E_{corr} value decreased with increasing the hydrostatic pressure, while i_{corr} decreased with increasing the hydrostatic pressure and R_p values increased with increasing the hydrostatic pressure. The decrease of i_{corr} and the increase of R_p mean the decrease of the overall corrosion rate. As shown in Table 4, the anodic Tafel slopes values increase with increasing the hydrostatic pressure, which indicates the anodic reaction is suppressed by the hydrostatic pressure. The change in the cathodic Tafel slopes is small, which indicates the cathodic reaction is less affected by the hydrostatic pressure. But the corrosion resistance of the steels is also related to the degree of pitting corrosion.

Table 4. Electrochemical parameters obtained from polarization curves of X65 steel after 12 h of erosion-corrosion in 3.5 mass% NaCl solution at different hydrostatic pressures.

Hydrostatic pressure (atm)	E_{corr} (mV_{SCE})	i_{corr} (10^{-6} A/cm^2)	R_p (Ω cm^2)	β_α (mV/ decade)	βc (mV/ decade)
1	-821	21.45	1761.5	175.9	123.5
5	-892	19.01	2115.9	231.4	128.6
10	-904	16.99	2099.9	300.2	132.7

Figure 8 shows the SEM morphologies of X65 steel samples under erosion-corrosion environment at different hydrostatic pressures. As shown in Fig. 8, the surface damage of the samples is aggravated by applying the hydrostatic pressure. Under one atmosphere pressure, as shown in Fig. 8a, the surface of the sample after erosion-corrosion testing showed uniform corrosion with some corrosion shallow pits (marked by the arrows). When the hydrostatic pressure was increased to five atmosphere pressure, the surface of the sample occurred serious local failure, showing some large and deep corrosion pits. As shown in Fig. 8b, in the corrosion pits, some micro-cracks were observed (marked by the arrows). When the hydrostatic pressure was increased to ten atmosphere pressure, as shown in Fig. 8c, the surface damage morphology of the sample is similar to that of the sample at 5 atm. The damage area of the sample at 10 atm is more larger than that of the sample at 5 atm (marked by the arrows). The fracture and shedding of corrosion products are accelerated by applying hydrostatic pressure, which indicates hydrostatic pressure accelerate the local failure of the sample during erosion-corrosion. Thus, although the overall corrosion current density of the sample was decreased after applying a certain hydrostatic pressure, its local damage degree was increased with pressure.

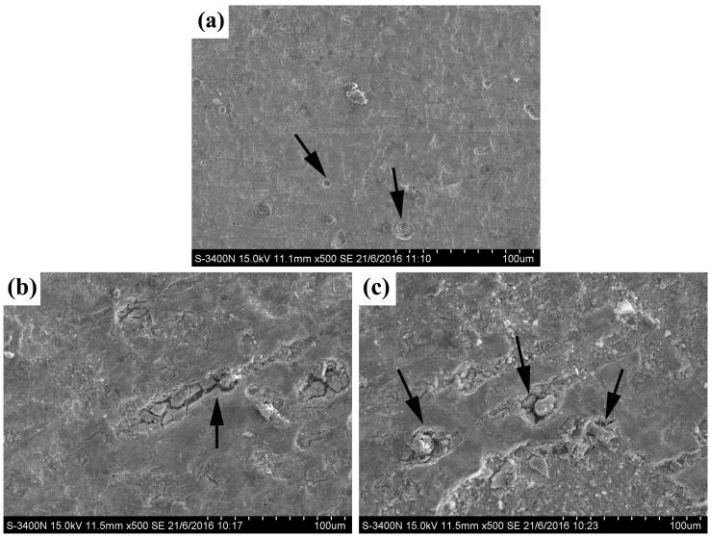

Figure 8. SEM morphologies of X65 steel after 12 h of erosion-corrosion in 3.5mass% NaCl solution at different hydrostatic pressures: (a) 1 atm; (b) 5 atm; (c) 10 atm.

Table 5 shows the main elements composition and their average content in the corrosion pits of the different samples. As shown in Table 5, it is noted that the Cl content in the corrosion pits of the sample increases with increasing its hydrostatic pressure. Cl^- is the primary aggressive ion which can accelerate pitting corrosion in seawater environment [11]. According to Beccaria and some other researchers [14, 21, 22], the transport of Cl^- was promoted by attaching the hydrostatic pressure, which increased the electrical conductivity of the corrosion product layer and enhanced the adsorption of the Cl^- to the metal substrate. Thus, the acceleration of local damage after applying pressure is due to the enhanced permeation of Cl^- to the metal substrate under high pressure.

Table 5. Main elements composition and their average content in the corrosion pits of X65 steel after 12 h of erosion-corrosion in 3.5 mass% NaCl solution at different hydrostatic pressures.

Element Atomic (%)	Hydrostatic pressure (atm)		
	1	5	10
O	49.493	56.295	64.222
Cl	0.730	2.689	3.768
Cr	2.559	0.365	0.097
Fe	46.727	40.495	31.469
Co	0.371	0.119	0.435
Ni	0.080	0.038	0.009
	100.000	100.000	100.000

Figure 9 shows the EIS curves of X65 steel after 12 h of test in 3.5 mass% NaCl solution at different pressures with a rotating speed of 100 rpm, which are in a similar shape. The similar shape of the EIS curves (Fig. 9) and the same corrosion type (Fig. 8) of the different samples indicates their

equivalent circuit model can be described as $R_s(Q_{dl}(R_t(Q_fR_f)))$, which is shown in Fig. 9. In the equivalent circuit model, R_s is the solution resistance, R_t is the charge transfer resistance of the uniform corrosion, Q_{dl} and Q_f is the constant phase element, and R_f is the charge transfer resistance of the pitting corrosion.

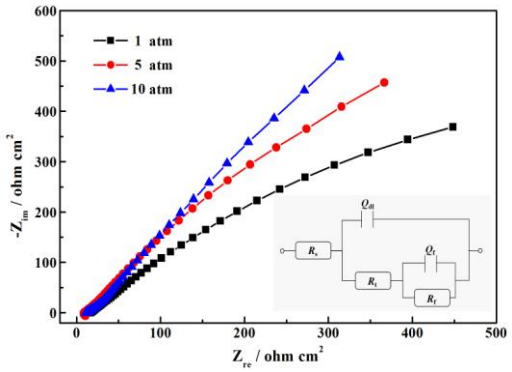

Figure 9. Nyquist plots of X65 steel after 12 h of erosion-corrosion in 3.5 mass% NaCl solution at different hydrostatic pressures with a rotating speed of 100 rpm.

Table 6 shows the R_t and R_f values of X65 steel under different pressures fitted by using ZSimpWin software. The higher R_t means the lower uniform corrosion rate of the whole surface. The lower R_f means the higher pitting corrosion rate of the local surface. As shown in Table 6, the R_t value of the sample under erosion-corrosion at 1 atm is about 1498 ohm cm^2, and its R_f value is 778 ohm cm^2. The R_t value of the sample increases with increasing the hydrostatic pressure, which indicates the additional hydrostatic pressure weaken uniform corrosion. The decreased uniform corrosion by applying pressure is mainly due to the retardative effect of the hydrostatic pressure to the mass transport process of ferric ion.

The R_f value of the sample decreases with increasing the hydrostatic pressure, which indicates the additional hydrostatic pressure accelerate local corrosion. The increased local damage by applying pressure is mainly due to the enhanced permeation process of Cl^- to the steel substrate. Thus, the hydrostatic pressure has the opposite effect on the uniform and local corrosion of X65 steel, showing a decrease of uniform corrosion and a increase of local failure.

Table 6. EIS parameters of the samples under different hydrostatic pressures.

Hydrostatic pressure (atm)	R_t (ohm cm^2)	R_f (ohm cm^2)
1	1498	778
5	1717	21.1
10	2318	14.9

4. CONCLUSION

A simple rotating experimental setup with adjustable rotating speed and hydrostatic pressure was established to simulate the erosion-corrosion environment. The effect of rotating speed and hydrostatic pressure on the erosion-corrosion behavior of X65 steel in 3.5 mass% NaCl was investigated.

Rotating speed changed the corrosion type of X65 steel under static state environment from a pure uniform electrochemical corrosion into the combination of uniform corrosion and local damage. Both the uniform corrosion and local damage of X65 steel was aggravated with increasing the rotating speed due to the synergistic damage effect of corrosion and erosive force.

The hydrostatic pressure has the opposite effect on the uniform and local corrosion of X65 steel, showing a decrease of uniform corrosion and a increase of local failure. The decreased uniform corrosion was mainly due to the retarded mass transport process of ferric ion by pressure. The increased local damage was mainly due to the enhanced permeation process of Cl^- to the steel substrate by pressure.

ACKNOWLEDGMENTS
This work was financially supported by the Natural Science Foundation of Guangdong Province China (2015A030310162) and the Science and Technology Plan of Guangdong Province China (2016A010103034).

References

1. D. M. Ortega-Toledo, J. G. Gonzalez-Rodriguez and M. Casales, *Int. J. Electrochem. Sci*., 6 (2011) 778.
2. G. A. Zhang, L. Y. Xu and Y. F. Cheng, *Corros. Sci*., 51 (2009) 283.
3. D. M. López, N. A. Falleiros and A. P. Tschiptschin, *Mat. Res.*, 19 (2016) 451.
4. H. X. Guo, B. T. Lu and J. L. Luo, *Electrochim. Acta*, 51 (2005) 315.
5. G. J. Bignold, *J. Mod. Power Syst. Cle*., 25 (2005) 11.
6. B. R. Tian and Y. F. Cheng, *Corros. Sci*., 50 (2008) 773.
7. X. Tang, L.Y. Xu and Y. F. Cheng, *Corros. Sci*., 50 (2008) 1469.
8. G. A. Zhang and Y. F. Cheng, *Corros. Sci.*, 51 (2009) 901.
9. X. Hu and A. Neville, *Wear*, 258 (2005) 641.
10. A. S. Hamdy, A. G. Sa'Eh and M. A. Shoeib, *Electrochim. Acta*, 52 (2007) 7068.
11. T. Zhang, Y. Yang and Y. Shao, *Electrochim. Acta*, 54 (2009) 3915.
12. Wang Z, Cong Y and Zhang T, *Int. J. Electrochem. Sci*., 9 (2014) 778.
13. A. M. Beccaria and G. Poggi, *Br. Corros. J*., 20 (1985) 183.
14. H. Sun, L. Liu and Y. Li, *J. Electrochem. Soc*., 160 (2013) 6177.
15. Y. Yang, T. Zhang and Y. Shao, *Corros. Sci*., 52 (2010) 2697.
16. J. Wang, J. Chen and B. Chen, *Tribol. Int*., 56 (2012) 38.
17. G. D. Eyu, G. Will and W. Dekkers, *Appl. Surf. Sci.*, 357 (2015) 506.
18. R. Vera, F. Vinciguerra and M. Bagnara, *Int. J. Electrochem. Sci*., 10 (2015),6187.
19. Covino, S. Bernard Jr. and D. Stephen, ASM Handbook, Corrosion, 9th ed., ASM International (1987) United States.
20. Z. B. Zheng and Y. G. Zheng, *Corros. Sci.*, 102 (2016) 259.

21. K. Fushimi and M. Seo, *J. Electrochem. Soc*., 380 (2011) 31.
22. A. M. Beccaria, G. Poggi and G. Castello, *Br. Corros. J*., 30 (1995) 283.